Article

Not peer-reviewed version

Exploring Gluconamide-Modified Silica Nanoparticles of Different Sizes as Effective Carriers for Antimicrobial Photodynamic Therapy

Ruth Prieto-Montero *, Lucia Herrera , Maite Tejón , Andrea Albaya , Jose Luis Chiara , Mónica L. Fanarraga , Virginia Martínez-Martínez *

Posted Date: 29 October 2024

doi: 10.20944/preprints202410.2336.v1

Keywords: Antimicrobial Resistance; Photosensitizer; Photodynamic Therapy; Silica nanoparticles; Rose Bengal; Gram negative; gluconamide; biotargeting

Article

Exploring Gluconamide-Modified Silica Nanoparticles of Different Sizes as Effective Carriers for Antimicrobial Photodynamic Therapy

Ruth Prieto-Montero [1,*], Lucia Herrera [1], Maite Tejón [1], Andrea Albaya [1,2], Jose Luis Chiara [2], Mónica L. Fanarraga [3] and Virginia Martinez-Martinez [1,*]

[1] Departamento de Química Física, Universidad del País Vasco-EHU, Facultad de Ciencia y Tecnología, Apartado 644, 48080 Bilbao, Spain
[2] Instituto de Química Orgánica General (IQOG-CSIC), Juan de la Cierva 3, 28006 Madrid, Spain
[3] Grupo de Nanomedicina Instituto de Investigación Valdecilla-IDIVAL, Universidad de Cantabria, Herrera Oria s/n, CP 39011 Santander, Spain
* Correspondence: ruth.prieto@ehu.eus (R.P.-M.); virginia.martinez@ehu.eus (V.M.-M.)

Abstract: Antimicrobial resistance (AMR), a consequence of the ability of microorganisms, especially bacteria, to develop resistance against conventional antibiotics hampering the treatment of common infections, is recognized as one of the most imperative health threats of this century. Antibacterial photodynamic therapy (aPDT) has emerged as a promising alternative strategy, utilizing photosensitizers activated by light to generate reactive oxygen species (ROS) that kill pathogens without inducing resistance. In this work, we synthesized silica nanoparticles of different sizes (20 nm, 80 nm, and 250 nm) functionalized with the photosensitizer Rose Bengal (RB) and a gluconamide ligand, which targets Gram-negative bacteria, to assess their potential in aPDT. Comprehensive characterization, including dynamic light scattering (DLS) and photophysical analysis, confirmed the stability and effective singlet oxygen production of the functionalized nanoparticles. RB loading was size-dependent, decreasing with increasing nanoparticle diameter. Consequently, the largest nanoparticles (250 nm) displayed insufficient RB surface density for effective aPDT, while the smallest (20 nm) and intermediate (80 nm) particles were more promising. Bacterial assays in *E. coli* revealed minimal dark toxicity and significant light-activated phototoxicity for the RB-loaded nanoparticles. The addition of gluconamide notably enhanced phototoxic activity, particularly in the smallest nanoparticles (RB-G-20@SiNP), which demonstrated the highest phototoxicity-to-cytotoxicity ratio. These findings indicate that small, gluconamide-functionalized silica nanoparticles are highly effective for targeted aPDT, offering a robust strategy to combat AMR.

Keywords: antimicrobial resistance; photosensitizer; photodynamic therapy; silica nanoparticles; Rose Bengal; gram negative; gluconamide; biotargeting

1. Introduction

Antimicrobial resistance (AMR) is a growing global health threat, underscored by the staggering statistic of 1.27 million annual deaths globally in 2019 directly attributed to infections caused by resistant microorganisms and nearly 5 millions deaths associated with resistant infections.[1–4]. The WHO further estimates that AMR could claim up to 10 million lives per year by 2050, and World Bank indicates it could lead to cumulative healthcare expenses of up to $1 trillion by that time [5,6]. AMR arises from the evolution of microorganisms, primarily Gram-negative bacteria that have acquired the ability to resist the effects of antibiotics. This resistance is often mediated by genetic changes, such as mutations or the acquisition of new genetic material, which enable bacteria to modify their structure or components, rendering them less susceptible to antibiotic action [1,7–10].

 doi:10.20944/preprints202410.2336.v1

Although new antibacterials are being developed, only a few of them can be considered as a new type. Besides, their implementation in the market is slow and their accessibility is limited, not reaching worldwide patients. Thus, non-traditional agents and treatments have to be explored as complements to antibiotics, from which the microorganism cannot develop resistance, to mitigate AMR.

Antimicrobial Photodynamic Therapy (aPDT) offers a promising alternative to conventional antibiotic treatments in the face of rising AMR. This therapeutic approach involves the use of a photosensitizer (PS), a light-sensitive molecule, in conjunction with light of a specific wavelength and intensity. Upon activation, the PS generates highly reactive reactive oxygen species (ROS), primarily singlet oxygen ($^1O_2$). These short-lived ROS species can effectively destroy cells, viruses, and bacteria, both directly and by disrupting their ability to transfer resistance genes to other microorganisms [11–19]. This rapid and localized action of aPDT helps to mitigate the spread of resistance, making it a valuable tool in combating the global AMR crisis. As the mechanism of action in PDT is rapid and local, it is crucial to precisely localize the PS in the infectious area. However, most of the available PSs (porphyrins, cyanines, xanthenes, BODIPYs, etc.)[18–22] do not present any special affinity for bacteria, being also accumulated inside normal cells and can induce side effects [18,20]. Besides, the hydrophobic nature of many photosensitizers limits their solubility in aqueous media, leading to the formation of molecular aggregates that considerably reduce the phototoxic action and, consequently, the effectiveness of PS.

In recent years, the use of nanoparticles (NP) has brought an important impact allied with overcoming the inherent PS limitations. The rational functionalization of the nanoparticle surface with targeting ligands makes them active vehicles for PS, increasing its selectivity, stability, biofilm penetration, solubility, and bioavailability in physiological media [23–31]. Nowadays, several types of nanoparticles, mainly lipid-based, are approved for their clinical use [32], and many others (polymeric and inorganic) are in (pre)clinical trials to evaluate their effectiveness and safety. This is the case for silica nanoparticles, which have entered clinical trials for a variety of biomedical applications [28,31,33–36]. Silica nanoparticles offer several advantages compared to organic nanoparticles, because of their excellent physicochemical properties (chemically inert, mechanically stable, optically transparent), their tuning structure (particle size and morphology, pore diameter), and surface functionality (as a consequence of a high presence of silanol groups on the surface) [37–43]. In this work, dense silica nanoparticles with different size diameters (25 nm, 80 nm, and 250 nm) were synthesized by the Stöber or arginine method [44,45]. The silica nanoparticles are externally functionalized with a commercial photosensitizer, Rose Bengal (RB), a very common PS with intense absorption band in the green region (λ_{abs} = 520-580 nm), modest fluorescence (Φ_{fl} = 10%) and high singlet oxygen production (Φ_{Δ} = 86%),[43,44] together with a targeting ligand for Gram-negative bacteria, a gluconamide derivative (G) (Figure 1). RB is used as a standard photosensitizer to elucidate the effect of the particle size of the gluconamide-modified and unmodified silica nanoparticles on the toxicity under dark and irradiated conditions in *E. coli* bacteria. This open-chain carbohydrate has demonstrated specific adhesion by favorable interaction with the bacteria lipopolysaccharide LPS outer membrane [46]. Additionally, the use of gluconamide coating hinders non-specific protein adhesion, the so-called protein corona formation, and reduces particle aggregation, increasing the stability of the nanosystem in the biological medium. The results of this study could be extended to other photosensitizers to expand the development of inexpensive, attainable, and efficient nanoplatforms for aPDT to combat AMR.

 doi:10.20944/preprints202410.2336.v1

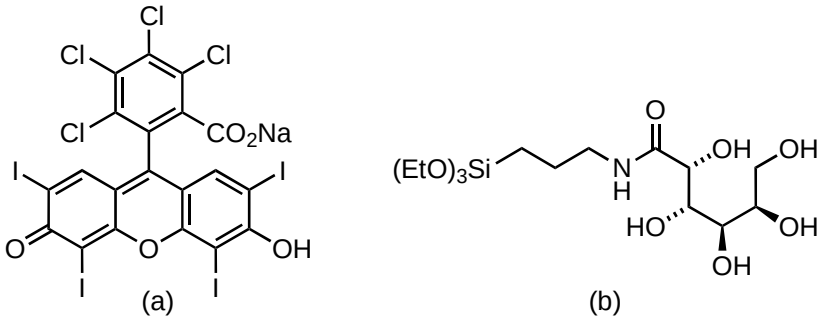

Figure 1. Molecular structures of Rose Bengal (a) and silylated-gluconamide derivative (b).

2. Materials and Methods

2.1. Materials

Tetraethoxysilane (TEOS, Sigma-Aldrich), ammonium hydroxide solution (28% NH_3, Sigma-Aldrich), arginine (Sigma-Aldrich), Rose Bengal (RB, Sigma-Aldrich), ethyl chloroformate (Across), triethylamine (Sigma-Aldrich), (3-aminopropyl)trimethoxysilane (APTMS, Sigma-Aldrich), *N*-(3-(triethoxysilyl)propyl)-D-gluconamide ("gluconamide", Gelest), were obtained from the indicated commercial sources.

2.2. Silica Nanoparticle Synthesis

2.2.1. Synthesis of 20 nm Silica NPs

To a solution of L-arginine (26.7 mg, 0.15 mmol) in H_2O (25 mL), TEOS (4 mL, 18 mmol) was added, and the mixture was stirred at 60 °C for 72 h. The resulting 20@SiNPs were washed with ethanol and water by centrifugation (15000 rpm = 21130 rcf, 1h) and then dried at 100 °C for 24 h.

2.2.2. Synthesis of 80 nm Silica NPs

NH_4OH (3.1 mL, 80 mmol) was added to a water-ethanol mixture (3.4 mL and 100 mL, respectively), and after stirring for 30 min, TEOS was added (3.8 mL, 17 mmol). The mixture was stirred at 27 °C for 24 h. The resulting 80@SiNPs were washed with ethanol and water by centrifugation (15000 rpm = 21130 rcf, 30 min) and dried at 100 °C for 24 h.

2.2.3. Synthesis of 250 nm Silica NPs

NH_4OH (8.4 mL, 174 mmol) was added to the water-ethanol mixture (6.4 mL and 40 mL, respectively), and after stirring for 30 min, TEOS was added (4.2 mL, 19 mmol). The mixture was stirred for 3 h at 58 °C. The resulting 250@SiNPs were washed with ethanol and water by centrifugation (15000 rpm = 21130 rcf, 30 min) and were dried at 100 °C for 24 h.

2.2.4. SiNP Functionalization with Rose Bengal and Gluconamide

A solution of Rose Bengal (26.4 mg, 0.026 mmol) in anhydrous methanol (20 mL) was stirred under a nitrogen atmosphere at 0 °C. Ethyl chloroformate (3 µL, 0.026 mmol) and triethylamine (4 µL, 0.026 mmol) were added dropwise. After further stirring for 30 minutes, (3-aminopropyl)trimethoxysilane (5 µL) was added to the reaction mixture, which was futher stirred for 1 h at 0 °C. Then, SiNP (30 mg), and *N*-(3-(triethoxysilyl)propyl)-D-gluconamide were added (11 µL, 0.026 mmol) and the mixture was mixed for 1 h at room temperature. The resultant suspension of fully functionalized SiNP with RB and gluconamide (named RB-G-20@SiNP, RB-G-80@SiNP, and RB-G-250@SiNP, for 20, 80 or 250 nm NPs size) was centrifuged (15000 rpm =21130 rcf) and washed with ethanol until a colorless supernatant was obtained. The RB-G@SiNP was collected by filtration (see Supporting Information, Scheme S1 and Figure S1). As a control sample, silica NP functionalized only

 doi:10.20944/preprints202410.2336.v1

with RB, without gluconamide (named RB-20@SiNP, RB-80@SiNP, and RB-G250@SiNP, respectively), were also synthesized.

2.3. Structural Characterization

The size, shape, and morphology of the obtained NPs were characterized by transmission electron microscopy (TEM) using a JEOL JEM 1400Plus operating at 100 kV. Images were acquired with a sCMOS Hamamatsu digital camera. Dynamic light scattering (DLS) and Zeta potential (ζ) measurements are performed in nanoparticle suspension (0.1 mg/mL) to analyze their hydrodynamic diameter and electrophoretic stability using a Malvern Zetasizer Nano ZS, which has a Helium-Neon (λ = 633 nm) laser. Elemental surface compositions (in atomic percentage, at%) of the silica nanoparticles were analyzed by X-ray photoelectron spectroscopy (XPS, SPECS equipment). The measurements were carried out by wide scan: energy step 0.1 eV, dwell time 0.1s, pass energy 30 eV with 901 electron exit angle.

2.4. Photophysical Characterization

The absorption spectra were recorded with a UV-Vis-NIR spectrometer (model Cary 7000, Agilent Technologies). In the case of the nanoparticle samples, an integrating sphere (model Internal DRA 900, Livingston, UK) was used for uniform light collection to correct the reflection and scattering effects of the samples. The fluorescence measurements were recorded with an Edinburgh Instruments Spectrofluorimeter (FLSP920 model, Livingston, UK) equipped with a 450 W xenon flash lamp as the excitation source. The fluorescence spectra were corrected from the wavelength dependence on the detector sensibility. The fluorescence quantum yields of the photosensitizers were measured by the relative method, using PM597 (Φ_{fl} = 0.48 in methanol) as the standard sample dye [47], following the equation:

$$\Phi_{fl} = \Phi_{fl}^{r} \frac{n^2}{(n^r)^2} \frac{(1-10^{A^r})}{(1-10^{A})} \frac{F}{F^r}$$

The singlet oxygen ($^1O_2$) production was determined by direct measurement of its phosphorescence at 1276 nm, Figure S2, employing an NIR detector (InGaAs detector, Hamamatsu G8605- 23), integrated into the same Edinburgh spectrofluorimeter upon continuous monochromatic excitation (450 W Xenon lamp) of the sample. Singlet oxygen quantum yields (Φ_{Δ}^{PS}) were calculated by the relative method, using commercial Rose Bengal (RB, Φ_{Δ}^{PS} = 0.86 in CD_3OD) [48] as reference, following equation:

$$\Phi_{\Delta}^{PS} = \Phi_{\Delta}^{R} \frac{S_e^{PS}}{S_e^{R}} \frac{\alpha^{R}}{\alpha^{PS}}$$

The amounts of RB attached to the external surface of silica NPs were estimated photometrically in RB@SiNPs stable suspensions, assuming the same molar extinction coefficients for the RB in solution and covalently attached to the silica surface.

2.5. Antibacterial Activity

Recombinant *E. coli* bacterial strains, engineered to overexpress a green fluorescent protein (GFP) mutant protein in the presence of isopropyl β-D-1-thiogalactopyranoside (IPTG) described elsewhere [49], were utilized to specifically identify viable bacteria by observing the production of GPF fluorescence. The protocol followed to expose the bacteria to the RB in solution or RB@SiNPs is depicted in Scheme S2. Briefly, the bacterial precultures were regrown until they reached an optical density (OD) of 0.6. A total of 750 µL of these cultures were re-suspended in PBS. For light exposure, 50 µL aliquots of this *E. coli* suspension were placed in the wells of a 24-well plate, followed by the addition of various solutions of RB or dispersions of PS@SiNP. To ensure an even distribution of the added compounds, the plate was vigorously shaken at 250 rpm for 30 minutes before irradiation. Irradiations were performed using light-emitting diode devices: LED Par 64 Short Q4-18 (Showtec, Burgebrach, Holland) in the green region (wavelength centered at 518 nm) as shown in Scheme S2.

 doi:10.20944/preprints202410.2336.v1

The total light dosage for green light irradiation (TLD) was previously optimized for the RB system [50] by varying the exposition time: from 30 min (16 J/cm^2) to 120 min (65 J/cm^2), being the total light dosage set at 65 Jcm^{-2} and it was the one used in this work.

To assess bacterial viability post-treatment, *E. coli* bacterial suspensions were subjected to serial dilution, with 100 μL of each dilution plated onto LB agar plates (see Scheme S23 and Figure S3). These plates were then incubated overnight at 37 °C, after which the number of viable bacteria was determined by counting the colony-forming units (CFU). This count was compared to the untreated control group. Each condition was replicated three times, and each experiment was conducted on three separate days. Bacterial survival is expressed as the percentage relative to the control CFU count (under dark conditions). Statistical differences between the control and treated *E. coli* were assessed using a *t*-test through the GraphPad Prism program. The significance level grade is: *P* value: * < 0.033, ** < 0.002, *** < 0.0002, and **** < 0.0001, $n = 3$, $DF = 4$.

2.6. Bacteria Imaging

For transmission electron microscopy (TEM) imaging of bacteria and nanoparticles, 150 μL of bacterial suspension, with OD = 0.6, were incubated with RB-G-20@SiNP, RB-G-80@SiNP or RB-G-250@SiNP (0.15 mg/mL) in PBS. After 2 hours of incubation, the bacteria were fixed in 4% paraformaldehyde for 20 minutes and washed with water four times. The samples were deposited on carbon-coated copper grids. Imaging was performed using Philips SuperTwin, CM200 at 200 kV, with LaB_6 filament applying different magnifications.

3. Results

3.1. Silica Nanoparticles Characterization

Silica nanoparticles with diameters of 20 nm, 80 nm, and 250 nm were selected to investigate the effect of particle size on antimicrobial photodynamic therapy (PDT). The success of these syntheses was confirmed by TEM and DLS, Figure 2, Figure S4, and Table 1. The three samples show spherical shapes with a narrow size distribution, Figure S4 and Table 1, being 21±2 nm for the 20@SiNPs, 80±5 nm for the 80@SiNPs, and 260±27 nm for 250@SiNPs. These values are consistent with the hydrodynamic diameter measured for 80@SiNPs and 250@SiNPs (0.1 mg/mL water suspension) by DLS (Table 1). However, 20@SiNPs, which are the smallest in size, showed a larger hydrodynamic diameter, sugggesting possible particle interaction in suspension. Regarding water stability, the ζ-potential values, higher than ±25 mV in the three samples, indicate good stabilities of the suspension in water and a low tendency to form larger aggregates [51]. The surface composition of these nanomaterials was studied by XPS (Table 1, and Figure S5). XPS spectra show the characteristic signals of Si (2p) at 102.5 eV and O (1s) at 523 eV, with a relative ratio 1: 2. The noisy signal assigned to C (1s) is of around 2-3 % and is assigned to adventitious carbon.

Table 1. Silica nanoparticle size by TEM and Dynamic Light Scattering (DLS), ζ-potential (ζ), and surface atomic composition (XPS) for the different samples.

Samples	TEM (nm)	DLS (nm)	ζ (mV)	XPS		
				%C	%O	%Si
20@SiNP	21±2	50	-31	2.8	68.8	28.3
80@SiNP	80±5	100	-33	3.1	63.0	33.9
250@SiNP	260±27	250	-53	2.0	70.1	27.9

 doi:10.20944/preprints202410.2336.v1

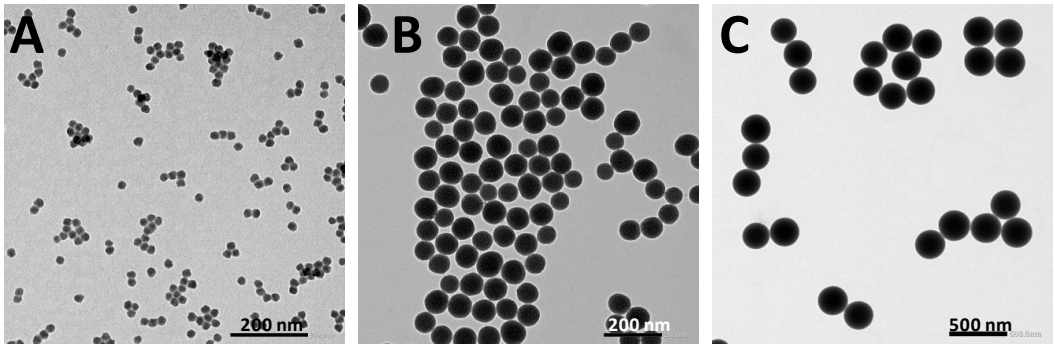

Figure 2. TEM images of 20@SiNPs, 80@SiNPs, and 250@SiNPs suspended in water (Scale bar 200 nm in A and B and 500 nm in C).

3.2. Silica Nanoparticles Post-Functionalization

The nanoparticles with different sizes (20, 80, and 250 nm) were externally functionalized with Rose Bengal, affording RB-20@SiNP, RB-80@SiNP, and RB-250@SiNP, respectively. The nanosystem were further modified with the gluconamide ligand, yielding RB-G-20@SiNP, RB-G-80@SiNP, and RB-G-250@ SiNP, respectively, Figure S1. The sequential addition of RB and G induces changes in the ζ-potential values. The hydrophobic character of the organic RB dye decreases ζ-potential by approximately 10 mV (less negative values), which is practically restored after the subsequent introduction of the hydrophilic gluconamide derivative, ensuring good stability of the nanosystems in water (Table 2). In contrast, the hydrodynamic diameter is not significantly affected by the presence of RB and G on the external surface (Table 2).

The amount of RB externally attached is quantified by the photometric method, recording the absorption spectra of the nanoparticles in suspension (Figure 3, Table 2). The amount of dye per gram covalently attached to the external silica surface, using the same functionalization conditions, is inversely proportional to the particle size (Table 2) in accordance with the decrease of surface-area-to-volume ratio with increasing volume. As a result, the estimated RB amount for RB-G-20@SiNP is 7 μmol/g, higher than that of RB-G-80@SiNP (2.1 μmol/g) and one order of magnitude larger than in RB-G-250@SiNP (0.8 μmol/g). Consequently, RB-G-20@SiNP and RB-G-80@SiNP could be considered suitable candidates to be implemented in aPDT. In contrast, the RB-G-250@SiNP nanosystem, with RB tethered at the outer surface of the nanoparticle at a low loading of 0.8 μmol/g, is less promising.

Table 2. Dynamic Light Scattering (DLS) size and ζ-potential (ζ), and RB loading for the different nanosystems.

Samples	DLS (nm)	ζ (mV)	[RB] μmol/g
RB-20@SiNP	41	-22	7.0
RB-G-20@SiNP	45	-29	7.0
RB-80@SiNP	81	-23	2.1
RB-G-80@SiNP	83	-40	2.1
RB-250@SiNP	261	-44	0.8
RB-G-250@SiNP	280	-46	0.8

The absorption and emission spectra of the three completed nanosystems reveal very similar features to the RB in solution, in position and shape (Figure 3 and Table 3), indicating the absence of dye aggregation at the nanoparticle surface. Besides, the photophysical properties in terms of fluorescent and singlet oxygen quantum yields are similar to RB in methanolic solution keeping a

 doi:10.20944/preprints202410.2336.v1

modest fluorescence efficiency ($\Phi_{fl} \geq 0.05$) and high singlet oxygen production ($\Phi_{\Delta} > 0.75$) for RB-G-20@SiNP and RB-G-80@SiNP (Table 3). In particular, RB-G-20@SiNP demonstrated the best photophysical properties together with the higher PS loaded at the nanoparticle, suggesting this sample is the most promising for aPDT.

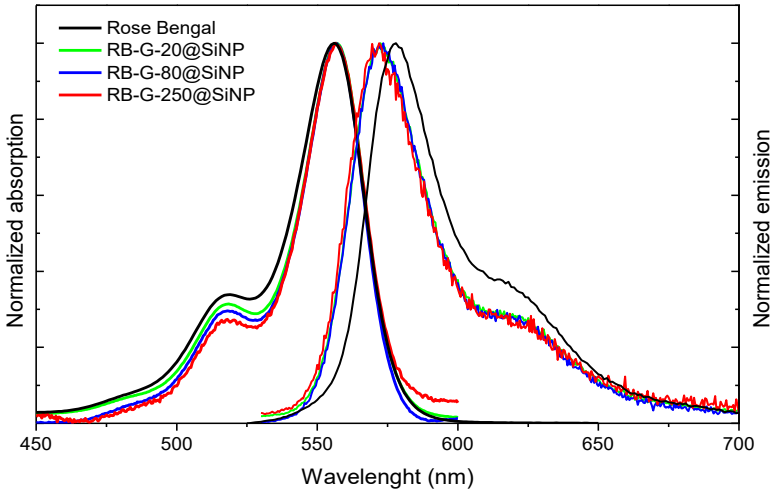

Figure 3. Normalized absorption and emission spectra of RB (black), RB-G-20@SiNP (green), RB-G-80@SiNP (blue) and RB-G-250@SiNP (red) in methanol.

Table 3. Photophysical properties of the complete samples: absorption (λ_{ab}) and fluorescence (λ_{fl}) wavelength, and fluorescence (Φ_{fl}), and singlet oxygen (Φ_{Δ}) quantum yield.

Samples	λ_{ab} (nm)	λ_{fl} (nm)	Φ_{fl}	Φ_{Δ}
RB	556	578	0.10	0.86
RB-G-20@SiNP	557	572	0.07	0.84
RB-G-80@SiNP	557	573	0.05	0.76
RB-G-250@SiNP	557	576	0.02	0.70

3.3. Antimicrobial Studies with Gram-Negative Bacteria?

Illustrative TEM images of the three nanosystems, RB-G-20@SiNP, RB-G-80@SiNP, and RB-G-250@SiNP incubated with *E. coli* bacteria were taken (Figure 4). TEM images reveal a very good adhesion of the three gluconamide-decorated silica nanosystems to the external wall of the *E. coli* bacteria. Fewer nanoparticles are located on the bacterial outer membrane in the case of RB-G-250@SiNP due to their larger size, which probably hinders interaction with the external LPS layer of the bacterial membrane. Combined with the previously mentioned low RB loading, higher nanoparticle concentrations (mg/mL) are required to achieve the desired RB concentration. Therefore,, this sample is discarded for the bio-assays in *E. coli*. To evaluate the potential of functionalized silica nanoparticles as a novel platform for aPDT against Gram-negative bacteria, we investigated the cytotoxicity and phototoxicity of nanoparticles with varying sizes (20 nm and 80 nm) and surface modifications (with and without gluconamide targeting ligand). Our study aimed to compare the activity of these nanoparticle-based aPDT systems to that of the photosensitizer RB in solution. Additionally, we explored the influence of the gluconamide ligand on the phototoxic efficacy of the nanoparticles, seeking to understand how this modification might enhance their antibacterial activity.

 doi:10.20944/preprints202410.2336.v1

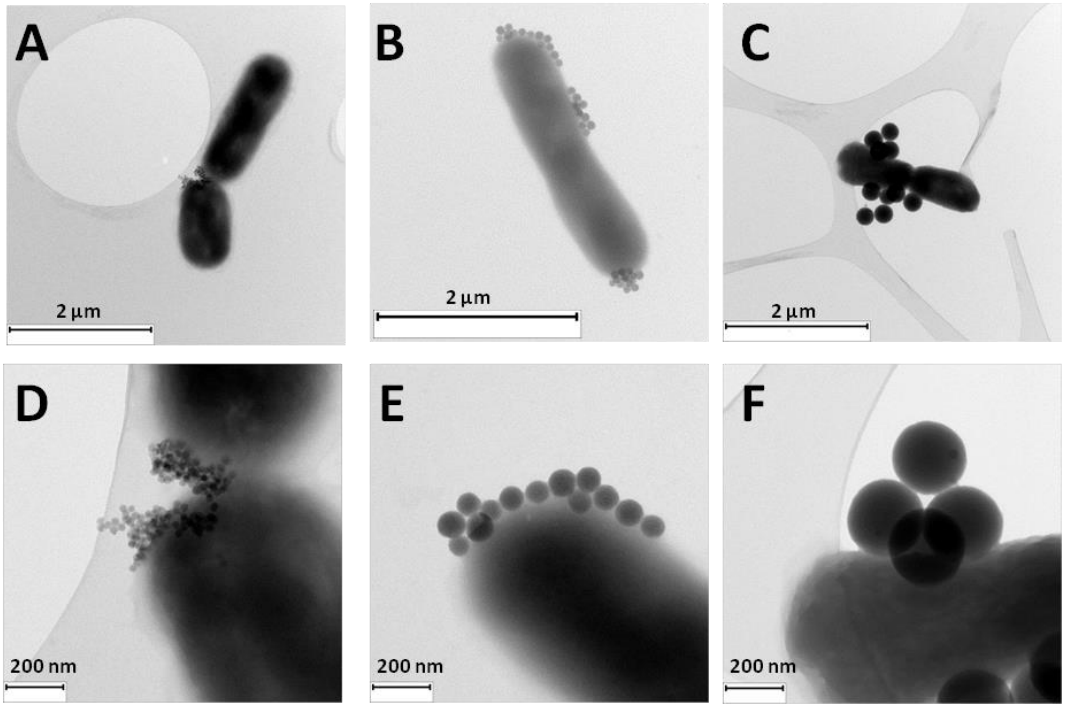

Figure 4. Representative TEM images of a fixed *E. coli* bacteria exposed to RB-G-20@SiNP(A, D), RB-G-80@SiNP (B, E), and RB-G-250@SiNP (C, F) at 0.15 mg/mL.

The viability studies of these nanoparticles in *E. coli* bacteria were carried out under dark and green irradiation. In our previous work, the protocol was optimized for RB in solution, setting the concentration at $5 \cdot 10^{-7}$ M and irradiation dose of 65 J/cm^2. It was also confirmed that the green irradiation source had a negligible cytotoxic effect on bacteria throughout the incubation period [50].

The four systems, RB-20@SiNP, RB-G-20@SiNP, RB-80@SiNP, and RB-G-80@SiNP, were tested in *E. coli* under dark conditions and green irradiation, and their performance was compared with free RB in solution (Figure 5). RB in solution displayed the highest phototoxicity, leading to the lowest % CFU (12%) with the largest grade of significance (****) compared to the bacterial control. However, this high phototoxicity is partly assisted by the cytotoxicity under dark conditions, which already leads to approximately 60% bacterial death. Although the reason for the RB intrinsic cytotoxicity in solution under dark conditions is not yet fully understood, previous studies showed that it increases with the incubation time or photosensitizer concentration, possibly as a consequence of the membrane permeabilization process by RB molecules [52,53].

A different scenario is observed for the photosensitized nanosystems (Figure 5). In dark conditions, the cytotoxicity of the four nanosystems is totally mitigated, with 96-99% CFU remaining viable, except for RB-20@SiNP, which induces a slight bacteria death (83% of CFU are alive). In these cases, RB is not able to cross the bacteria membrane as it is covalently linked to SiNPs, and accordingly, dark toxicity from RB is avoided.

The photoactivity of the four nanosystems, RB-20@SiNP, RB-G-20@SiNP, RB-80@SiNP, and RB-G-80@SiNP, resulted in a bacterial viability range of 25-50 % CFU. There are significant differences for those systems functionalized with gluconamide moiety. For instance, RB-20@SiNP and RB-80@SiNP lead to 35% and 48% CFU, with ** and no grade of significance when compared to the dark control, respectively. However, their homologous nanosystems with gluconamide, RB-G-20@SiNP, and RB-G-80@SiNP, reach 27% and 34% CFU, respectively with *** grade of significance in both cases, which represent an increase in the phototoxicity under green irradiation when compared with those without the targeting ligand. Besides, RB-G-20@SiNP has completely reduced the dark cytotoxicity, which was not the case for RB-20@SiNP.

These results confirm the critical role of gluconamide targeting on the nanoparticle surface in enhancing phototoxicity while preventing dark cytotoxicity. This effect is likely due to the

 doi:10.20944/preprints202410.2336.v1

improvement of the stability of nanoparticles in water avoiding aggregation, according to the ζ-potential results (Table 2), and the favorable interaction between nanoparticles and the bacterial cell wall, proposed in previous studies [46].

Regarding the size effect of the silica NPs, both the 20 nm and 80 nm nanosystems, show promising results against Gram-negative bacteria, with RB-G-20@SiNP demonstrating slightly better performance under green irradiated conditions.

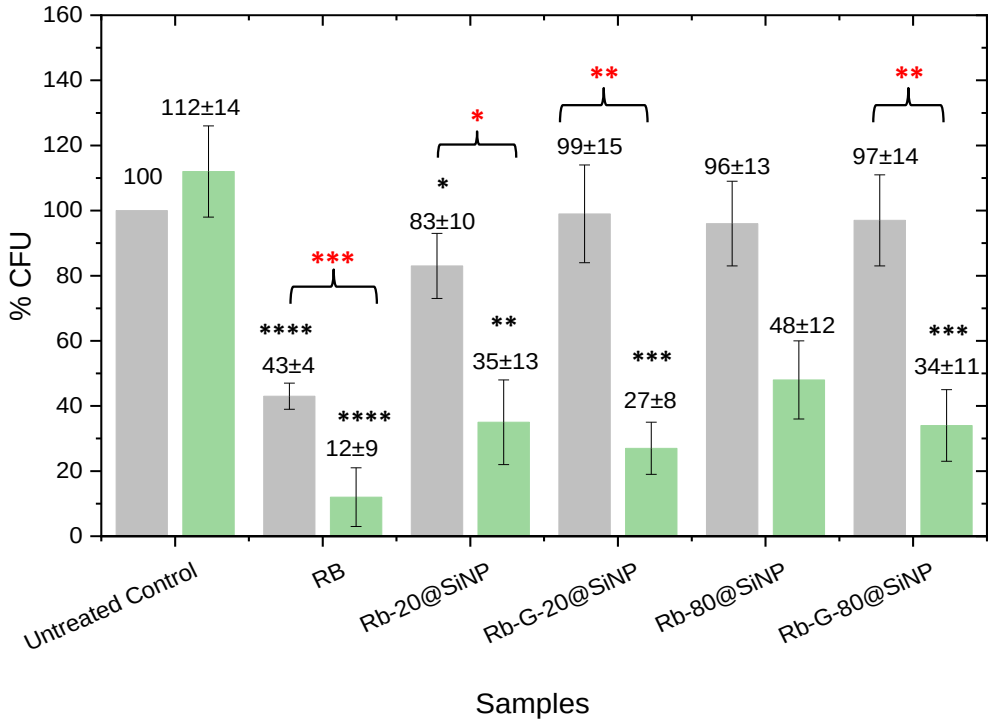

Figure 5. CFU % (as viability test) of *E. coli* bacteria in dark (grey bar) and under 2 hours of green irradiation (green bar) incubated with samples normalized at $5 \cdot 10^{-7}$ M concentration of RB. Black asterisks indicate a significant difference compared to controls. Red asterisks indicate significant differences between dark and light conditions in the same sample tested. *P* value: * < 0.033, ** < 0.002, *** < 0.0002, and **** < 0.0001, $n = 3$, $DF = 4$.

5. Conclusions

Silica nanoparticles of different sizes (20 nm, 80 nm, and 250 nm), externally functionalized with commercial RB as photosensitizer and gluconamide as specific biotargeting ligand for Gram Negative, were synthesized as promising candidates for aPDT. All nanosystems were thoroughly characterized and evaluated in *E. coli*.

DLS measurements confirmed good stability of the systems in aqueous media, particularly after covalent functionalization with gluconamide. The photophysical properties of RB attached to the silica nanoparticles were similar to those for RB in diluted solution, showing modest fluorescence and high singlet oxygen production, indicative of minimal dye aggregation. RB loading on the nanoparticle surface decreased with increasing particle size, with the largest (250 nm) nanoparticles showing an order of magnitude lower RB loading compared with the smallest (25 nm) ones, making RB-250@SiNP sample not suitable for aPDT.

Our bacterial assay revealed that the use of silica nanoparticles as carriers for RB effectively minimized the intrinsic cytotoxicity of the photosensitizer under dark conditions. Additionally, the presence of a gluconamide targeting moiety on the nanoparticle surface significantly enhanced the phototoxic activity of the photosensitized nanosystems. Notably, the smallest nanoparticle size, RB-G-20@SiNP, demonstrated the highest ratio of phototoxicity to cytotoxicity, closely followed by the intermediate-sized nanocarrier RB-G-20@SiNP. These findings underscore the potential of silica

 doi:10.20944/preprints202410.2336.v1

nanoparticles, particularly those with a gluconamide targeting moiety and smaller size, as promising platforms for antimicrobial photodynamic therapy.

In conclusion, our study highlight that small silica nanoparticles fully functionalized with RB and a gluconamide targeting moiety represent a promising nanoplatform for aPDT. These nanosystems offer an efficient photoactivated treatment with minimal dark toxicity, ensuring safety during administration. Future work will explore the potential of other photosensitizers to further optimize the efficacy and versatility of this approach in combating antimicrobial resistance.

Supplementary Materials: The following supporting information can be downloaded at the website of this paper posted on Preprints.org. Scheme S1. Schematic representation of silica nanoparticles functionalization with RB and Gluconamide; Scheme S2: Irradiation protocol for E. coli exposure; Figure S1. Images of original Silica nanoparticles, RB-G-20@SiNP, RB-G-80@SiNP, and RB-G-250@SiNP; Figure S2. Representative singlet oxygen emission spectra for sample RB-G-25@SiNP and reference Rose Bengal excited at 550 nm; Figure S3. Overnight cultures of *E. coli* after serial dilutions for cell counting; Figure S4: TEM images and size distribution of 20@SiNPs, 80@SiNPs , and 250@SiNPs according to TEM images. Figure S5. XPS spectra of Si 2p, O 1s and C 1s for SiO2 nanoparticles of 20nm, 80 nm, and 250 nm.

Author Contributions: Ruth Prieto-Montero: Writing – original draft, Methodology, Investigation. Maite Tejón: Methodology, Investigation. Lucia Herrera: Methodology, Andrea Albaya: Methodology. Jose Luis Chiara: Writing – review & editing, Project administration, Investigation, Funding acquisition. Mónica L. Fanarraga: Writing – review & editing, Supervision, Methodology, Investigation, Funding acquisition. Virginia Martínez-Martínez: Writing – review & editing, Supervision, Project administration, Investigation, Funding acquisition, Data curation, Conceptualization.

Funding and Acknowledgments: This work was funded by MCIN/AEI/10.13039/501100011033 (projects PID2020- 114347RB-C32 and PID2020-114347RB-C31, to VMM and JLC, respectively) and European Union NextGenerationEU/PRTR (projects TED2021-129248B-I00 to MLF, and TED2021-132122B-C22 to JLC and VMM), Gobierno Vasco-Eusko Jaurlaritza (project IT1639-22) to VMM, and Spanish Instituto de Salud Carlos iii (projects PI22/00030) to MLF. RP-M, and MT, thank MIU and NGEU for the postdoctoral contract (MARSA21/71), and Investigo program funding (EU-Next generation), respectively. AA thanks MCIN for a predoctoral contract (PRE2021-098894).

Acknowledgments: We would like to thank the Advanced Research Facilities (SGIker) of the University of the Basque Country for technical and human support.

Conflicts of Interest: The authors declare no conflicts of interest.

References

1. Samreen; Ahmad, I.; Malak, H.A.; Abulreesh, H.H. Environmental antimicrobial resistance and its drivers: a potential threat to public health. *Journal of Global Antimicrobial Resistance* **2021**, *27*, 101–111.
2. Songca, S.P.; Adjei, Y. Applications of Antimicrobial Photodynamic Therapy against Bacterial Biofilms. *International Journal of Molecular Sciences* **2022**, *23*, 3209.
3. Cassini, A.; Högberg, L.D.; Plachouras, D.; Quattrocchi, A.; Hoxha, A.; Simonsen, G.S.; Colomb-Cotinat, M.; Kretzschmar, M.E.; Devleesschauwer, B.; Cecchini, M.; Ouakrim, D A.; Oliveira, T. C.; Struelens, M. J.; Suetens, C.; Monnet, D. L.; the Burden of AMR Collaborative Group. Attributable deaths and disability-adjusted life-years caused by infections with antibiotic-resistant bacteria in the EU and the European Economic Area in 2015: a population-level modelling analysis. *The Lancet Infectious Diseases* **2019**, *19*, 56–66.
4. Ran, B.; Wang, Z.; Cai, W.; Ran, L.; Xia, W.; Liu, W.; Peng, X. Organic Photo-antimicrobials: Principles, Molecule Design, and Applications. *Journal of the American Chemical Society* **2021**, *143*, 17891–17909.
5. Murray, C.J.L.; Ikuta, K.S.; Sharara, F.; Swetschinski, L.; Robles Aguilar, G.; Gray, A.; Han, C.; Bisignano, C.; Rao, P.; Wool, E.; Antimicrobial Resistance Collaborators. Global burden of bacterial antimicrobial resistance in 2019: a systematic analysis. *The Lancet* **2022**, *399*, 629–655.
6. *Drug-Resistant Infections*; World Bank, Washington, DC, 2017;
7. Laxminarayan, R.; Matsoso, P.; Pant, S.; Brower, C.; Røttingen, J.-A.; Klugman, K.; Davies, S. Access to effective antimicrobials: a worldwide challenge. *The Lancet* **2016**, *387*, 168–175.

8. Tacconelli, E.; Carrara, E.; Savoldi, A.; Harbarth, S.; Mendelson, M.; Monnet, D.L.; Pulcini, C.; Kahlmeter, G.; Kluytmans, J.; Carmeli, Y.; Cox, E. M.; Houchens, C. R.; Grayson, M. L.;Hansen, P.; Singh, N.; Theuretzbacher, U.; Magrini, N.; the WHO Pathogens Priority List Working Group. Discovery, research, and development of new antibiotics: the WHO priority list of antibiotic-resistant bacteria and tuberculosis. *The Lancet Infectious Diseases* **2018**, *18*, 318–327.
9. Jørgensen, P.S.; Wernli, D.; Carroll, S.P.; Dunn, R.R.; Harbarth, S.; Levin, S.A.; So, A.D.; Schlüter, M.; Laxminarayan, R. Use antimicrobials wisely. *Nature* **2016**, *537*, 159–161.
10. Schrader, S.M.; Vaubourgeix, J.; Nathan, C. Biology of antimicrobial resistance and approaches to combat it. *Science Translational Medicine* **2020**, *12*, 1–14.
11. Yin, R.; Hamblin, M. Antimicrobial Photosensitizers: Drug Discovery Under the Spotlight. *Current Medicinal Chemistry* **2015**, *22*, 2159–2185.
12. Mula, S.; Koli, M. Helical BODIPY Dyes as Heavy-Atom-Free Triplet Photosensitizers for Photodynamic Therapy of Cancer. *ChemMedChem* **2024**, *19*, 1–7.
13. Lin, J.; Wan, M.T. Current evidence and applications of photodynamic therapy in dermatology. *Clinical, Cosmetic and Investigational Dermatology* **2014**, *7*, 145–163.
14. Moghissi, K.; Dixon, K.; Gibbins, S. A Surgical View of Photodynamic Therapy in Oncology: A Review. *The Surgery Journal* **2015**, *01*, e1–e15.
15. Sarbadhikary, P.; George, B.P.; Abrahamse, H. Recent advances in photosensitizers as multifunctional theranostic agents for imaging-guided photodynamic therapy of cancer. *Theranostics* **2021**, *11*, 9054–9088.
16. Triesscheijn, M.; Baas, P.; Schellens, J.H.M.; Stewart, F.A. Photodynamic Therapy in Oncology. *The Oncologist* **2006**, *11*, 1034–1044.
17. Hu, X.; Huang, Y.Y.; Wang, Y.; Wang, X.; Hamblin, M.R. Antimicrobial photodynamic therapy to control clinically relevant biofilm infections. *Frontiers in Microbiology* **2018**, *9*, 1–24.
18. Correia, J.H.; Rodrigues, J.A.; Pimenta, S.; Dong, T.; Yang, Z. Photodynamic Therapy Review: Principles, Photosensitizers, Applications, and Future Directions. *Pharmaceutics* **2021**, *13*, 1332.
19. DeRosa, M.; Crutchley, R.. Photosensitized singlet oxygen and its applications. *Coordination Chemistry Reviews* **2002**, *233–234*, 351–371.
20. Mfouo-Tynga, I.S.; Dias, L.D.; Inada, N.M.; Kurachi, C. Features of third generation photosensitizers used in anticancer photodynamic therapy: Review. *Photodiagnosis and Photodynamic Therapy* **2021**, *34*, 102091.
21. Prieto-Montero, R.; Prieto-Castañeda, A.; Sola-Llano, R.; Agarrabeitia, A.R.; García-Fresnadillo, D.; López-Arbeloa, I.; Villanueva, A.; Ortiz, M.J.; Moya, S.; Martínez-Martínez, V. Exploring BODIPY Derivatives as Singlet Oxygen Photosensitizers for PDT. *Photochemistry and Photobiology* **2020**, *96*, 458–477.
22. Kamkaew, A.; Lim, S.H.; Lee, H.B.; Kiew, L.V.; Chung, L.Y.; Burgess, K. BODIPY dyes in photodynamic therapy. *Chemical Society reviews* **2013**, *42*, 77–88.
23. Deng, J.; Yang, M.; Li, C.; Liu, G.; Sun, Q.; Luo, X.; Wu, F. Single molecular-based nanoparticles with aggregation-induced emission characteristics for fluorescence imaging and efficient cancer phototherapy. *Dyes and Pigments* **2021**, *187*, 109130–109137.
24. Qiao, Y.; Geng, H.; Jiang, N.; Zhu, X.; Li, C.; Cai, Q. Polymyxin B–modified upconversion nanoparticles for selective detection of Gram-negative bacteria such as Escherichia coli. *Journal of Chemical Research* **2020**, *44*, 756–761.
25. Guzel Kaya, G.; Medaglia, S.; Candela-Noguera, V.; Tormo-Mas, M.Á.; Marcos, M.D.; Aznar, E.; Deveci, H.; Martínez-Máñez, R. Antibacterial Activity of Linezolid against Gram-Negative Bacteria: Utilization of ε-Poly-l-Lysine Capped Silica Xerogel as an Activating Carrier. *Pharmaceutics* **2020**, *12*, 1126.

26. Lucky, S.S.; Soo, K.C.; Zhang, Y. Nanoparticles in Photodynamic Therapy. *Chemical Reviews* **2015**, *115*, 1990–2042.
27. Kabanov, V.; Press, D.J.; Huynh, R.P.S.; Shimizu, G.K.H.; Heyne, B. Assessment of encapsulated dyes' distribution in silica nanoparticles and their ability to release useful singlet oxygen. *Chemical Communications* **2018**, *54*, 6320–6323.
28. Prieto-Montero, R.; Arbeloa, T.; Martínez-Martínez, V. Photosensitizer-Mesoporous Silica Nanoparticles Combination for Enhanced Photodynamic Therapy (PDT). *Photochemistry and Photobiology* **2023**, *99*, 882–900.
29. Abdel Gaber, S.A.; Stepp, H.; Abdel Kader, M.H.; Lindén, M. Mesoporous silica nanoparticles boost aggressive cancer response to hydrophilic chlorin e6-mediated photodynamic therapy. *Cancer Nanotechnology* **2023**, *14*, 67.
30. Mangalath, S.; Saneesh Babu, P.S.; Nair, R.R.; Manu, P.M.; Krishna, S.; Nair, S.A.; Joseph, J. Graphene Quantum Dots Decorated with Boron Dipyrromethene Dye Derivatives for Photodynamic Therapy. *ACS Applied Nano Materials* **2021**, *4*, 4162–4171.
31. Simões, J.C.S.; Sarpaki, S.; Papadimitroulas, P.; Therrien, B.; Loudos, G. Conjugated Photosensitizers for Imaging and PDT in Cancer Research. *Journal of Medicinal Chemistry* **2020**, *63*, 14119–14150.
32. Anselmo, A.C.; Mitragotri, S. Nanoparticles in the clinic: An update post COVID-19 vaccines. *Bioengineering and Translational Medicine* **2021**, *6*, 1–20.
33. Anselmo, A.C.; Mitragotri, S. Nanoparticles in the clinic: An update. *Bioengineering & Translational Medicine* **2019**, *4*, 1–16.
34. Aflakian, F.; Mirzavi, F.; Aiyelabegan, H.T.; Soleimani, A.; Gholizadeh Navashenaq, J.; Karimi-Sani, I.; Rafati Zomorodi, A.; Vakili-Ghartavol, R. Nanoparticles-based therapeutics for the management of bacterial infections: A special emphasis on FDA approved products and clinical trials. *European Journal of Pharmaceutical Sciences* **2023**, *188*, 106515.
35. Janjua, T.I.; Cao, Y.; Yu, C.; Popat, A. Clinical translation of silica nanoparticles. *Nature Reviews Materials* **2021**, *6*, 1072–1074.
36. Yang, Y.; Zhang, M.; Song, H.; Yu, C. Silica-Based Nanoparticles for Biomedical Applications: From Nanocarriers to Biomodulators. *Accounts of Chemical Research* **2020**, *53*, 1545–1556.
37. Singh, P.; Srivastava, S.; Singh, S.K. Nanosilica: Recent Progress in Synthesis, Functionalization, Biocompatibility, and Biomedical Applications. *ACS Biomaterials Science and Engineering* **2019**, *5*, 4882–4898.
38. Gubala, V.; Giovannini, G.; Kunc, F.; Monopoli, M.P.; Moore, C.J. Dye-doped silica nanoparticles: synthesis, surface chemistry and bioapplications. *Cancer Nanotechnology* **2020**, *11*, 1.
39. Shahabi, S.; Treccani, L.; Rezwan, K. A comparative study of three different synthesis routes for hydrophilic fluorophore-doped silica nanoparticles. *Journal of Nanoparticle Research* **2016**, *18*, 28.
40. Pallavi, P.; Harini, K.; Alshehri, S.; Ghoneim, M.M.; Alshlowi, A.; Gowtham, P.; Girigoswami, K.; Shakeel, F.; Girigoswami, A. From Synthetic Route of Silica Nanoparticles to Theranostic Applications. *Processes* 2022, *10*, 2595.
41. Ma, D.; Kell, A.J.; Tan, S.; Jakubek, Z.J.; Simard, B. Photophysical Properties of Dye-Doped Silica Nanoparticles Bearing Different Types of Dye−Silica Interactions. *The Journal of Physical Chemistry C* **2009**, *113*, 15974–15981.
42. Bouramtane, S.; Bretin, L.; Pinon, A.; Leger, D.; Liagre, B.; Richard, L.; Brégier, F.; Sol, V.; Chaleix, V. Porphyrin-xylan-coated silica nanoparticles for anticancer photodynamic therapy. *Carbohydrate Polymers* **2019**, *213*, 168–175.

43. Wang, Z.; Hong, X.; Zong, S.; Tang, C.; Cui, Y.; Zheng, Q. BODIPY-doped silica nanoparticles with reduced dye leakage and enhanced singlet oxygen generation. *Scientific Reports* **2015**, *5*, 12602.
44. Stöber, W.; Fink, A.; Bohn, E. Controlled growth of monodisperse silica spheres in the micron size range. *Journal of Colloid and Interface Science* **1968**, *26*, 62–69.
45. Watanabe, R.; Yokoi, T.; Kobayashi, E.; Otsuka, Y.; Shimojima, A.; Okubo, T.; Tatsumi, T. Extension of size of monodisperse silica nanospheres and their well-ordered assembly. *Journal of Colloid and Interface Science* **2011**, *360*, 1–7.
46. Capeletti, L.B.; de Oliveira, J.F.A.; Loiola, L.M.D.; Galdino, F.E.; da Silva Santos, D.E.; Soares, T.A.; de Oliveira Freitas, R.; Cardoso, M.B. Gram-Negative Bacteria Targeting Mediated by Carbohydrate–Carbohydrate Interactions Induced by Surface-Modified Nanoparticles. *Advanced Functional Materials* **2019**, *29*, 1–11.
47. Bañuelos Prieto, J.; López Arbeloa, F.; Martínez Martínez, V.; Arbeloa López, T.; López Arbeloa, I. Photophysical Properties of the Pyrromethene 597 Dye: Solvent Effect. *The Journal of Physical Chemistry A* **2004**, *108*, 5503–5508.
48. Prieto-Montero, R.; Prieto-Castañeda, A.; Katsumiti, A.; Cajaraville, M.P.; Agarrabeitia, A.R.; Ortiz, M.J.; Martínez-Martínez, V. Functionalization of Photosensitized Silica Nanoparticles for Advanced Photodynamic Therapy of Cancer. *International Journal of Molecular Sciences* **2021**, *22*, 6618–6641.
49. García-Hevia, L.; Saramiforoshani, M.; Monge, J.; Iturrioz-Rodríguez, N.; Padín-González, E.; González, F.; González-Legarreta, L.; González, J.; Fanarraga, M.L. The unpredictable carbon nanotube biocorona and a functionalization method to prevent protein biofouling. *Journal of Nanobiotechnology* **2021**, *19*, 1–13.
50. Prieto-Montero, R.; Tejón, M.; Albaya, A.; Arbeloa, T.; Chiara, J.L.; Fanarraga, M.L.; Martínez-Martínez, V. Targeted photodynamic therapy: Gluconamide-modified cellulose nanocrystals as efficient photosensitizer delivery platforms against Gram-negative bacteria. *Carbohydrate Polymers* **2024**, *3*, 122784.
51. Arulprakasajothi, M.; Elangovan, K.; Chandrasekhar, U.; Suresh, S. Performance study of conical strip inserts in tube heat exchanger using water based titanium oxide nanofluid. *Thermal Science* **2018**, *22*, 477–485.
52. Atrash, M.; Hovor, I.; Gurianov, Y.; Barel, M.; Semenova, O.; Brider, T.; Nisnevitch, M.; Nakonechny, F. Antibacterial Properties of Rose Bengal Conjugated to Hyaluronic Acid. *International Journal of Molecular Sciences* **2024**, *25*.
53. Kurosu, M.; Mitachi, K.; Yang, J.; Pershing, E. V.; Horowitz, B.D.; Wachter, E.A.; Lacey, J.W.; Ji, Y.; Rodrigues, D.J. Antibacterial Activity of Pharmaceutical-Grade Rose Bengal: An Application of a Synthetic Dye in Antibacterial Therapies. *Molecules* **2022**, *27*.